Theoretical and Applied Climatology (2021) 144:1407–1418
https://doi.org/10.1007/s00704-021-03609-w

ORIGINAL PAPER

Drought monitoring and evaluation using ESA CCI and GLDAS-Noah soil moisture datasets across China

Gengxi Zhang [1,2] · Xiaoling Su [1,2] · Olusola O. Ayantobo [3,4] · Kai Feng [1,2]

Received: 21 September 2020 / Accepted: 30 March 2021 / Published online: 12 April 2021

Abstract

Soil moisture (SM) plays a fundamental role in governing the water and energy balance at land-atmosphere interfaces and in controlling plant growth and biological interactions, which makes it a key indicator in drought identification. We compared and evaluated two types of surface SM datasets (Global Land Data Assimilation System-Noah-simulated (GLDAS-Noah); Europe Space Agency's Climate Change Initiative (ESA CCI)) for drought analysis in China over 1979–2014. The cumulative density function (CDF) matching method was employed to fill the data gap of ESA CCI data using the GLDAS-Noah SM products. Drought characteristics of duration, severity, and frequency were appraised on a grid basis using the Standardized Soil Moisture Index (SSI). The results show that the SSI values calculated based on these two SM products are significantly correlated ($p < 0.05$) over most parts (70%) of China, with similar patterns of average drought duration, severity, and frequency. The duration and severity at the arid and semiarid regions (with duration over 3 months; with an average severity of −3.1) are generally higher than those over humid regions (with the duration of 2 months; with an average severity of −2.7), but both SM datasets show higher drying trends in humid regions. However, the two SM datasets exhibit large discrepancies in the spatial patterns of drought duration, severity, and frequency trends, especially in arid and cold regions. Both SM products are capable of monitoring extreme drought events reported in southwestern, southern, and northern China compared with the Standardized Precipitation Index (SPI). Overall, both data sources have the potential to be used for drought monitoring; however, caution should be paid in high altitude and latitude regions where a large discrepancy exists.

Keywords Drought · Soil moisture · ESA CCI · GLDAS-Noah · China

1 Introduction

Drought is a creeping recurrent natural hazard that adversely influences agricultural productivity, human livelihoods, and ecosystems (Hao and Singh 2015; Chen et al. 2019). Generally, drought may last for months or years, extending from meteorological to agricultural and hydrological drought, causing severe natural disasters (Wilhite and Glantz 1985; McVicar and Jupp 1998; Yang et al. 2020). For example, the 2010 spring drought in southwestern China reduced winter wheat production by 48 and 31% in Yunnan and Guizhou provinces, respectively (Zhang et al. 2012). The 2011 summer drought in the Yangtze River basin cost approximately 2.4 billion US dollars (Jin et al. 2013; Yuan et al. 2015). Moreover, the 2019 severe drought in southern China affected several provinces, including Anhui, Hubei, Jiangsu, Jiangxi, and Zhejiang provinces, among which, Anhui province was the worst-affected region because it received about 60% less rainfall than normal between August and October (http://www.futuredirections.org.au/publication/southern-china-experiences-another-severe-drought/). To lessen drought damages, remote sensing (RS) techniques (Yuan et al. 2015; Rajasekaran et al. 2018; Blyverket et al. 2019) and land surface models (Mo and Lettenmaier 2014; Ayantobo and Wei

✉ Xiaoling Su
xiaolingsu@nwafu.edu.cn

1 College of Water Resources and Architectural Engineering, Northwest A&F University, Yangling 712100, China

2 Key Laboratory for Agricultural Soil and Water Engineering in Arid Area of Ministry of Education, Northwest A&F University, Yangling 712100, China

3 Department of Water Resources Management and Agricultural-Meteorology, Federal University of Agriculture, PMB 2240, Abeokuta 110282, Nigeria

4 State Key Laboratory of Hydroscience and Engineering, Department of Hydraulic Engineering, Tsinghua University, Beijing, China

2019; Zhang et al. 2019a) have been used for timely drought monitoring and analysis, especially in large regions.

Soil moisture (SM) is the key component of the earth system that dominates the water transport between soil, vegetation, and atmosphere and controls the water and energy balance, making it a fundamental indicator for drought monitoring, notably for agricultural drought (Brocca et al. 2011; Liu et al. 2019). SM data can be acquired from the measured sites, land surface models (LSM), and remote sensing. The measured site affords the most accurate point-based SM data with poor spatial representatives, however, due to the high costs of maintenance, and the measurement sites are globally sparse. Temporarily, most observation data are no longer adequate for drought monitoring and analysis (Robock et al. 2000).

In contrast, the LSMs can provide large spatial scale and long-term grid-based SM data with a high spatiotemporal resolution (Wang et al. 2016). However, the LSMs data quality depends heavily on the accuracy of the forcing variables, model parameters, and the model physical structures (Fang et al. 2016). The performance of LSMs in drought monitoring has large uncertainties with land surface complexity and climate variability (Levine et al. 2016). To address this issue, RS products have been utilized to adjust and merge LSMs data for SM monitoring and drought analysis (Liu et al. 2019; Zhang et al. 2019b; Vergopolan et al. 2020).

In the past two decades, a series of satellites have been launched for carrying a radiometer (passive) or radar (active) or both, providing band information for SM retrieval (Liu et al. 2012; Al-Yaari et al. 2019). These RS SM data are provided separately (e.g., Soil Moisture Active Passive (SMAP) (Entekhabi et al. 2010), Soil Moisture and Ocean Salinity (SMOS) (Kerr et al. 2001)) or blended (such as the one produced by the ESA project: Climate Change Initiative (CCI). Usually, microwave measurements are not affected by cloud contamination and varying solar illumination (Liu et al. 2019). Therefore, the SM data retrieved directly from these satellite observations are less affected by error accumulation, despite their thin penetration into the bare soil (<5 cm) (Spennemann et al. 2015). The microwave sensors-derived SM is closely related to that generated from the first layer in most LSMs. SM in shallow surface responds fast to meteorological anomalies (e.g., precipitation, evapotranspiration), serving as a sensitive indicator for drought monitoring. However, differences in sensor design, retrieval algorithms, terrain, and vegetation state could result in varying quality and inconsistency of the satellite data (Dorigo et al. 2015).

Many researchers have cross-validated different SM datasets under normal conditions (Brocca et al. 2011; Dorigo et al. 2012; Fang et al. 2016), but data quality shows more substantial variations in extreme conditions (e.g., drought). This could be due to the immature model structures and sparse forcing data for the LSMs and also high noise for the RS datasets (Taylor et al. 2012; Dorigo et al. 2015; Wang et al. 2016). These variations could plausibly influence SM drought monitoring. Therefore, the comparison of SM datasets could identify their consistencies and discrepancies and reveal their applicabilities in drought monitoring (Liu et al. 2019).

Among various SM data datasets, the GLDAS-Noah and the ESA CCI SM products have been widely applied for drought monitoring (Spennemann et al. 2015; Yuan et al. 2015; Zhang et al. 2019b). Therefore, we compare these two datasets for drought characterization across China and its respective characteristics. The objectives of this study include (i) to investigate the consistencies and discrepancies between these two datasets in monitoring droughts in different regions across China; (ii) to evaluate the capacity of the datasets in long-term drought monitoring; and (iii) to evaluate the capabilities of two datasets in drought detection during extreme droughts occurring.

2 Data

2.1 ESA CCI soil moisture

The ESA CCI Soil Moisture project (http://www.esasoilmoisture-cci.org) has been established to satisfy some needs based on passive and active microwave products in support of climate research (Dorigo et al. 2017). The latest release (v04.5) provides global soil moisture data from 1978 to 2018 with a spatial resolution of 0.25° × 0.25° and in units of m^3/m^3, merging three active (AMI-WS, MetOp-A ASCAT, and MetOp-BASCAT) and seven passive (SMMR, SSM/I, TMI, WindSat, AMSR-E, AMSR2, and SMOS) microwave products. The ESA CCI SM consists of three types (active, passive, and active-passive) of microwave products. The surface SM derived from the ESA CCI passive-active combined product was obtained from 1979 to 2014, and the monthly averaged ESA CCI SM values were subsequently computed for all grids across China.

2.2 GLDAS-Noah soil moisture

NASA Global Land Data Assimilation System Version 2 (GLDAS-2) has three components: GLDAS-2.0, GLDAS-2.1, and GLDAS-2.2. GLDAS-2.0 is forced entirely with the Princeton meteorological forcing input data and provides a temporally consistent series from 1948 through 2014 (Rodell et al. 2004; Beaudoing and Rodell 2019). The surface (0–10cm) SM data from GLDAS-2.0/Noah are used for drought analysis in this study.

2.3 Precipitation data

Monthly gridded precipitation data from 1979 to 2014, with a spatial resolution of 0.5° across China, were acquired from the

National Meteorological Information Center (NMIC) which is a department of the China Meteorological Administration (CMA) (http://data.cma.cn/). This dataset was generated using the thin plate spline (TPS) of ANUSPLIN software based on the observed precipitation data from 2472 ground stations in China from 1961 to the latest (McVicar and Jupp 1998). This dataset has been tested using the measured in situ precipitation data across China and showed very high precision (Zhao et al. 2014). The dataset was resampled to 0.25° resolution, as same as ESA CCI and GLDAS-Noah, using a bilinear interpolation method.

3 Methods

3.1 ESA CCI SM gap filling

The ESA CCI SM spans from 1978 to date, making it suitable for drought research (Brocca et al. 2011; Blyverket et al. 2019; Liu et al. 2019). However, the data gaps of the dataset hinder its application (Yuan et al. 2015). Therefore, for each pixel, we filled the missing values with GLDAS-Noah SM data, using the cumulative distribution function (CDF) matching approach (Reichle 2004; Drusch 2005; Brocca et al. 2011) as follows:

(1) Plotting the CDF curves of monthly ESA CCI SM and GLDAS-Noah SM, respectively.
(2) The polynomial regression is applied to GLDAS-Noah SM and the differences between ESA CCI and GLDAS-Noah SM.
(3) Match the CDF of GLDAS-Noah SM to ESA CCI SM, thereby yielding the GLDAS-CDF series (Fig. 1).

3.2 Standardized Precipitation Index (SPI)

The metrological drought was assessed for comparison, and it was evaluated using the monthly gridded precipitation data. Precipitation significantly and directly influences the SM, especially surface SM. Considering the instant response of shallow SM to precipitation (Szalai and Szinell 2000; Sims et al. 2002), 1-month SPI values were calculated in this study. The formula of SPI is bellowed (Mckee et al. 1993; Lloyd-Hughes and Saunders 2002; Liu et al. 2014):

$$SPI = \begin{cases} -\left(t - \dfrac{C_0 + C_1 t + C_2 t^2}{1 + d_1 t + d_2 t^2 + d_3 t^3}\right) & for \;\; 0 < H(x) \le 0.5 \\ t = \sqrt{\ln\left(1/H(x)^2\right)} & \\ t - \dfrac{C_0 + C_1 t + C_2 t^2}{1 + d_1 t + d_2 t^2 + d_3 t^3} & for \;\; 0.5 < H(x) < 1.0 \\ t = \sqrt{\ln\left(1/\left(1 - H(x)^2\right)\right)} & \end{cases} \tag{1}$$

where the coefficients C_0, C_1, C_2, d_1, d_2, and d_3 are given as follows: C_0=2.515517, C_1=0.802853, C_2=0.010328, d_1=1.432788, d_2=0.189269, and d_3=0.001308. $H(x)$ represents the cumulative probability, which is obtained from the Gamma CDF. One can refer to Ayantobo et al. (2017) for more details. Drought classification criteria are as shown in Table 1.

3.3 Drought identification

Droughts across China were characterized by the Standardized Soil Moisture Index (SSI) (Hao and AghaKouchak 2013; AghaKouchak 2014; Hao et al. 2014)

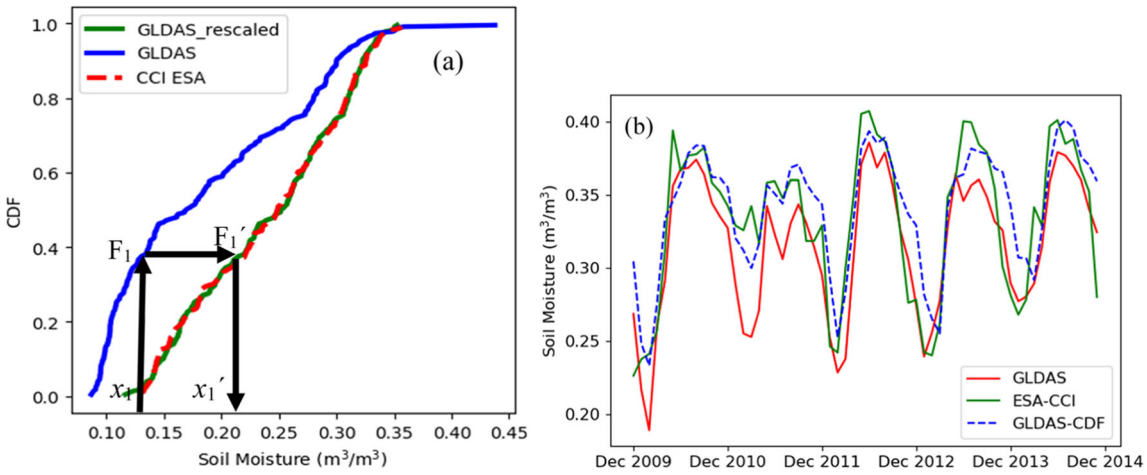

Fig. 1 Example of cumulative distribution function matching method (**a**) implemented to rescale GLDAS SM products, against ESA CCI SM data. The GLDAS-CDF product (**b**) is derived by applying a 5th-order polynomial fitting to the difference between the ranked GLDAS SM and ESA CCI SM data

Table 1 Drought classification criteria for soil moisture droughts (SSI) and meteorological droughts (SPI)

Drought category	SSI	SPI
No drought	>−0.5	>−0.5
Mild drought	−0.8 to −0.5	−1.0 to −0.5
Moderate drought	−1.3 to −0.8	−1.5 to −1.0
Severe drought	−1.6 to −1.3	−2.0 to −1.5
Extreme drought	−2.0 to −1.6	<−2.0
Exceptional drought	<−2.0	

from the ESA CCI SM and GLDAS-Noah datasets. The SSI can be calculated similarly to SPI (Mckee et al. 1993). The CDF is estimated using a nonparametric approach where the empirical probability (P) of the SM data is derived using the empirical Gringorten plotting position (Gringorten 1963). Then the P is transformed into a standard Gaussian distribution function, SSI = Φ^{-1}(P), where Φ is the standard Gaussian distribution function, and the greatest negative value of SSI represents the most severe drought. According to the SSI classification criteria (Hao et al. 2014), this study focused on the moderate (SSI<−0.8) and above grade droughts, which are referred to as droughts hereinafter.

3.4 SSI correlations

The correlations (R) of ESA CCI SM-derived SSI and GLDAS-Noah SM-derived SM were calculated for each calendar month at the pixel scale, using the formula given below:

$$r = \frac{n\sum_i SM_{ESAi}SM_{GLDASi} - \sum_i SM_{ESAi}\sum_i SM_{GLDASi}}{\sqrt{n\sum_i SM_{ESAi}{}^2 - \left(\sum_i SM_{ESAi}\right)^2}\sqrt{n\sum_i SM_{GLDASi}{}^2 - \left(\sum_i SM_{GLDASi}\right)^2}} \quad (2)$$

where SM_{ESAi} and SM_{GLDASi} represent the ith year's ESA CCI SM and the GLDAS-Noah SM.

3.5 Drought characterization and trend detection

In this paper, drought duration, frequency, and severity were calculated to determine their effectiveness for drought monitoring and analysis. Drought duration refers to the consecutive months where the drought index is below the truncation level. Drought frequency represents the reciprocal of the average drought interval in a given period, while drought severity refers to the cumulative sum of values during a drought period (Ayantobo et al. 2017)

The trends for SSI and the corresponding drought characteristics are examined utilizing the Mann-Kendall (M-K) method, a very popular method for trend identification (Dorigo et al. 2012; Liu et al. 2012). The M-K trend test defined as in Eq. 3 is used to quantify the significance of trends in the time series (Raziei 2017),

$$S = \sum_{i=1}^{n-1}\sum_{j=i+1}^{n} sign(x_j - x_i) \quad (3)$$

where x_i and x_j are the sequential data values in the time series ($j > i$) and n represents the length of the dataset. The $sign(x_j - x_i)$ is equal to 1, 0, or −1 when the resulting value is greater than, equal to, or less than zero, respectively. If the sample size n is greater than 30, the standard normal test statistic z can be computed to quantify the trend using Eq. 4:

$$z = \begin{cases} \frac{S-1}{\sqrt{Var(S)}} & if \ S > 0 \\ 0 & if \ S = 0 \\ \frac{S+1}{\sqrt{Var(S)}} & if \ S < 0 \end{cases} \quad (4)$$

where Var(S) is the variance of S, given by:

$$Var(S) = \frac{1}{18}\left[n(n-1)(2n+5) - \sum_t f_t(f_t-1)(2f_t+5)\right] \quad (5)$$

where t varies over the set of tied ranks and f_t is the number of times that the rank t appears. The M-K z-score was used to test the significance level for Gaussian distribution, with $p < 0.05$ representing a significant trend and vice versa.

3.6 Comparison with typical droughts

To evaluate the performances of these two SM datasets in drought monitoring, several historical droughts were chosen for drought comparison across China. These events consist of the 2010 spring drought in southwestern China (Zhang et al. 2012), the 2010–2011 severe winter drought in the North China Plain (Jin et al. 2013), and the 2011 summer drought in the middle and lower reaches of the Yangtze River basin of China (Yuan et al. 2015).

4 Results and discussion

4.1 SSI correlations between ESA CCI SM and GLDAS-Noah

Figure 2 shows R values between SSI values derived from ESA CCI and GLDAS-Noah, with the median, upper, and lower quartiles for each calendar month identified. In most cases, the R values are more than 0.2, and the median correlations are more than 0.4.

Figure 3 shows the R patterns of SSI for seasons and the whole year. The data gaps in ESA CCI, which could either be

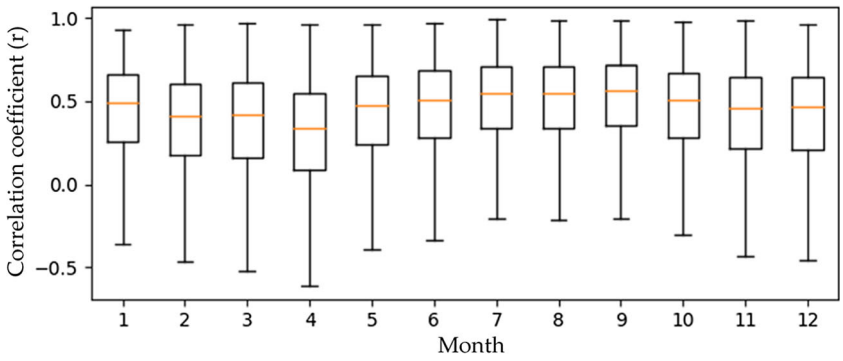

Fig. 2 Pearson's correlation coefficient (r) between the monthly SSI calculated using ESA CCI SM and GLDAS-Noah SM datasets for each calendar month over the study region

due to changing input sensor constellation or to natural physical phenomena (e.g., soil frost), lead to the missing R values in some regions (white blank). For the whole year, the significant R values dominate over 70% across China. Insignificant even negative correlations mainly appeared in the northwestern arid regions, Tibetan regions, and northeastern cold regions. This figure also shows that correlations vary with the season, with more significant correlations in more regions in warm seasons and lesser in cold seasons. For the entire month, the SSI calculated using ESA CCI SM showed good agreement with GLDAS-Noah SM data. The low correlations observed in the high latitude (northeastern China), high altitude (Tibet Plateau), and arid regions (Xinjiang and Inner Mongolia) were ascribed to the inability of sensors to obtain SM data in freeze-thaw zones (Dorigo et al. 2015) and large uncertainties of LSM in these regions (Ferguson and Wood

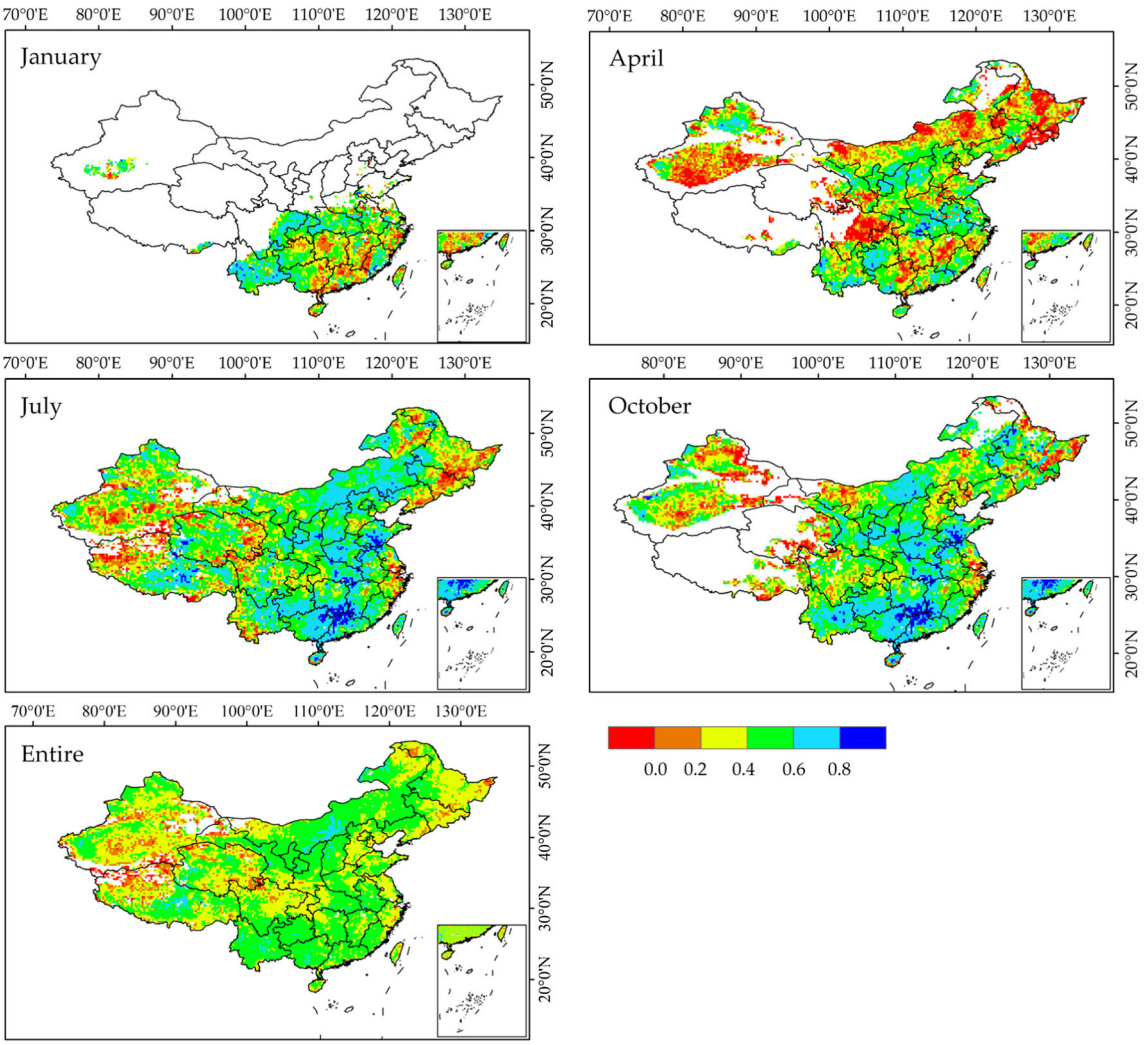

Fig. 3 Spatial distribution of Pearson's correlation coefficients between the SSI calculated using ESA CCI SM and GLDAS-Noah SM datasets for seasons and whole year over 1979–2014

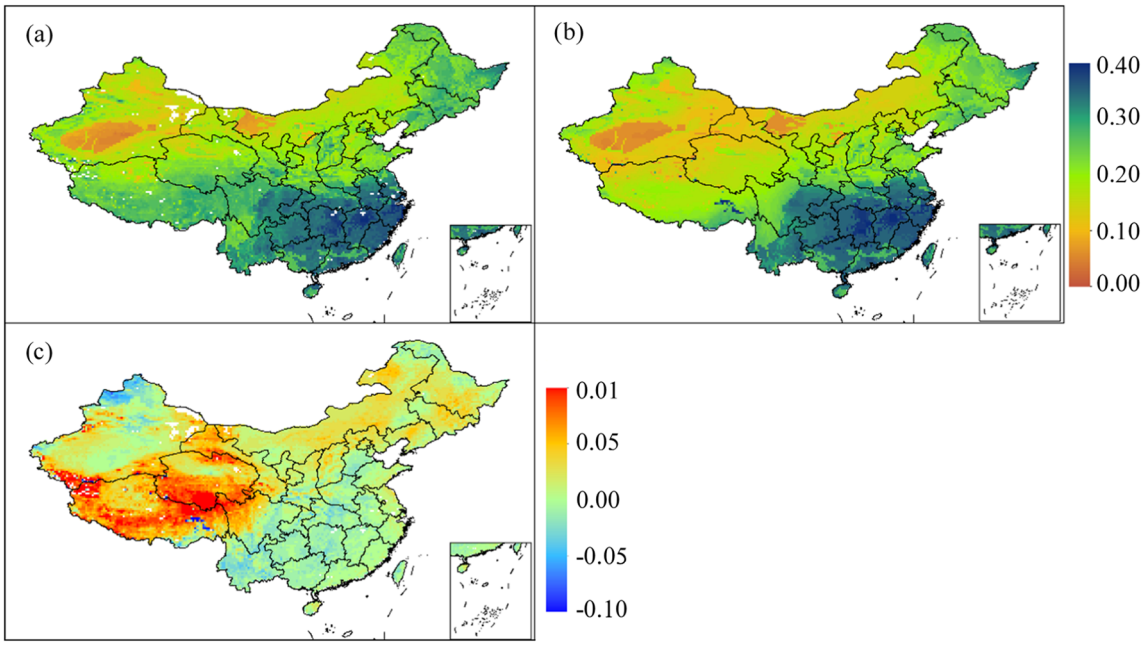

Fig. 4 Spatial distribution of surface soil moisture (m^3/m^3) for **a** the ESA CCI SM, **b** the GLDAS-Noah SM, and **c** their differences subtracting from the ESA CCI SM by the GLDAS-Noah SM

2011). The GLDAS outputs accuracy is controlled by inputs accuracy, parameters uncertainty, and feedback mechanisms for land-atmosphere (Ferguson and Wood 2011; Taylor et al. 2012; Liu et al. 2019). In northwestern arid regions and Tibetan, the gauge density for GLDAS model inputs (e.g., precipitation) is sparser than in other regions, which makes more errors and high uncertainty for model outputs. Besides, in freeze/thaw surface (Tibetan Plateau, and northeastern China), due to the physical limitations (frozen ground impacting the backscatter measurements), it is a challenging task to obtain accurate retrieval of SM from microwave measurements (Zwieback et al. 2015), in which the noise of satellite data may drown out the signal (Reichle 2004).

4.2 Assessment of drought characteristics

Figure 4 presents the spatial patterns of SM for ESA CCI and GLDAS-Noah and their averaged differences for the 1979–2014 period. Generally, the distribution patterns and values of the two datasets are in agreement, with SM values decreasing gradually from the southeast to the northwest. High SM (> 0.3 m^3/m^3) could be found in the humid and subhumid areas, while low SM (< 0.2 m^3/m^3) dominates the arid areas (Fig. 5). However, the ESA CCI SM was lower than GLDAS-Noah SM in humid and semi-humid regions (Fig. 5), while the ESA CCI SM was greater than GLDAS-Noah SM in other regions, especially in the Tibetan Plateau.

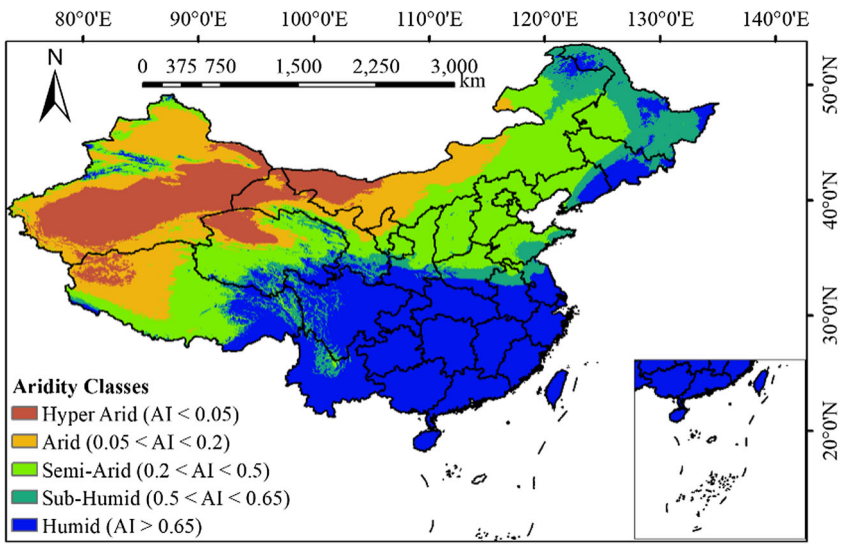

Fig. 5 China aridity map (from http://ref.data.fao.org/map?entryId=221072ae2090-48a1-be6f-5a88f061431a&tab=about). AI is an aridity index calculated by dividing the average yearly precipitation using the average yearly potential evapotranspiration

Figure 6 displays the patterns of averaged drought characteristics for the ESA CCI and the GLDAS-Noah SM over 1979–2014 for 1-month SSI. The spatial distribution of drought duration according to ESA CCI SM generally agreed with the GLDAS-Noah SM (Fig. 6a, b). According to our analysis, drought duration ranged from 1 to 4 months in the whole region. The durations over the arid and subarid regions are generally higher than that over the humid regions. Moreover, 82% of the regions have a duration of fewer than 2 months spreading over the humid regions (Fig. 5) for ESA CCI SM and 86% for GLDAS-Noah SM. Also, 52% of the region with a duration greater than 3 months are found in the arid regions (Fig. 5) for ESA CCI SM and 69% for GLDAS-Noah SM. Generally, the duration derived from GLDAS-Noah SSI was higher (for 81% total pixels) than that derived from ESA CCI SSI. The discrepancies in averaged drought duration are mainly found in the arid regions (southern Xinjiang, northern Tibetan Plateau) and some cold regions (eastern Inner Mongolia and Northeast).

The spatial distribution of drought severity is consistent with that of drought duration for the two datasets (Fig. 6c, d). Droughts were more severe over the arid regions (i.e., with an averaged severity of about −2.85 and −3.40 for ESA CCI and GLDAS-Noah, respectively) than that over the humid regions (i.e., with averaged severity of about −2.58 and −2.90 for ESA CCI SM and GLDAS-Noah datasets, respectively). Major discrepancies were also found in the arid regions.

The two datasets displayed a consistent spatial pattern of drought frequency. Drought events had a relatively higher frequency in the humid and semi-humid regions (i.e., with an averaged frequency of about 0.34 $month^{-1}$ and 0.37 $month^{-1}$ for ESA CCI and GLDAS-Noah, respectively) and relatively lower frequency in the arid regions (i.e., with an averaged frequency of about 0.35 $month^{-1}$ and 0.32 $month^{-1}$ for ESA CCI and GLDAS-Noah SM, respectively). This suggested that drought occurred more frequently but with shorter duration and slight severity in humid and semi-humid regions, while it occurred more severely with longer duration and relatively lower frequency in the arid region.

The obvious disparity for drought characteristics monitored by ESA CCI and GLDAS-Noah SM datasets mostly concentrated in arid (northwestern China) and cold regions (northeastern and Tibetan regions). This is due to the low signal-to-noise ratio for satellite SM over arid regions and high

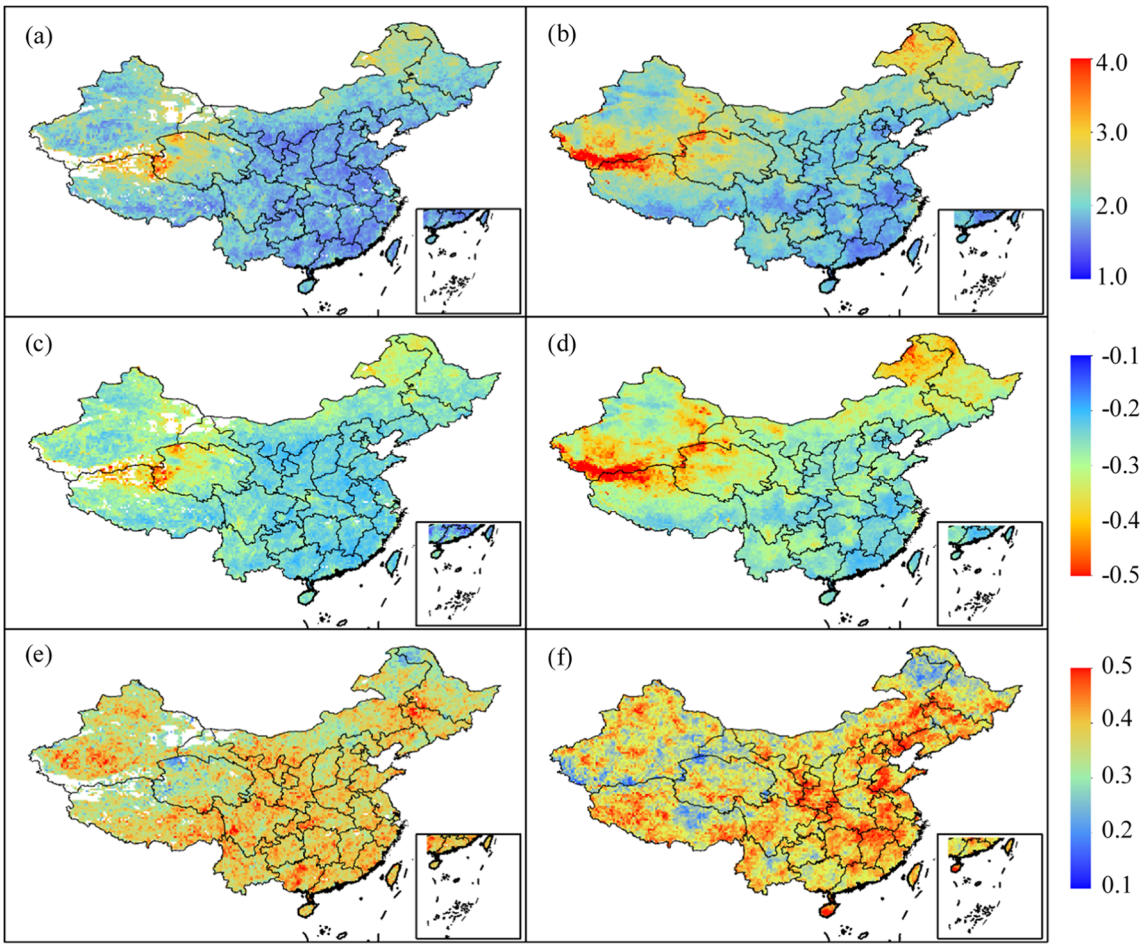

Fig. 6 Spatial distribution of averaged drought duration, severity, and frequency for the ESA CCI SM (**a**, **c**, **e**) and the GLDAS SM (**b**, **d**, **f**) over 1979–2014 based on SSI

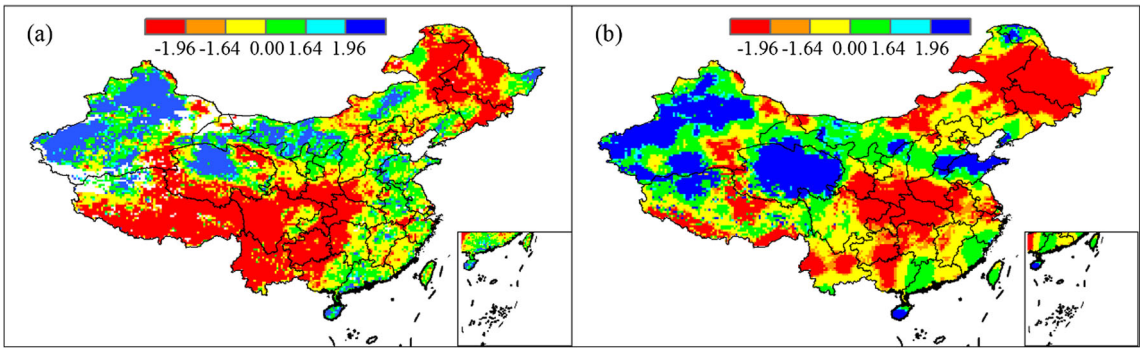

Fig. 7 Spatial distribution of trend significance (M-K z-score) in SSI for **a** ESA CCI SM and **b** GLDAS SM over 1979–2014

uncertainty in LSM in high altitude, freeze-thaw zones, and dry climate zones.

4.3 Drought trend detection

Long-term trends of SSI and corresponding drought characteristics between ESA CCI SM and GLDAS-Noah SM were compared using the M-K trend test method. Figure 7 shows the Mann-Kendall *z*-score in SSI for ESA CCI SM and GLDAS-Noah SM. Both two SM datasets showed similar spatial patterns with drying trends over central, southern, and eastern China and wetting trends over northwestern China. Accordingly, 35.8 and 16.7% of the regions showed a significant drying trend, while 16.7 and 17.5% of the regions presented a significant wetting trend for ESA CCI SM and GLDAS-Noah SM, respectively. According to our results, most of the above regions were found in the humid and semi-humid zone. The grid to grid consistent ratios of the significant drying and wetting trends between ESA CCI SM and GLDAS-Noah SM were ~18.1 and 10.0%, respectively, and major discrepancies in SSI trends between the two datasets are mainly located in southwestern China (Fig. 7).

To further understand drought changes, the average SSI was calculated over southwestern China (i.e., Yunnan, Sichuan, Guizhou, and South Tibet) monthly from 1979 through 2014 (Fig. 8). The SSI for ESA CCI SM showed a slight and insignificant increasing trend from 1979 to 1999, while after 2000, SSI decreases significantly (R^2=0.20, p < 0.01) with a change rate of −0.04/year (Fig. 8a). In contrast, the SSI for GLDAS-Noah SM had no obvious trend for the whole period (Fig. 8b). This showed that ESA CCI SM agreed well with GLDAS-Noah SM before 2000, but ESA CCI SM was generally lower than GLDAS-Noah SM between 2000 and 2014, especially in the winter season.

For drought duration, few pixels presented a significant drying trend (z-score > 1.96) for both two datasets (i.e., 7% for ESA CCI SM and 2% for GLDAS-Noah SM) (Fig. 9a, b). For the ESA CCI SM, major significant upward trends appeared in the humid and semi-humid regions, such as southwestern China, where drying trends had been previously detected (Liu et al. 2017). In the case of GLDAS-Noah SM, significant increasing (drying) trends appeared in some northeastern areas and parts of the central and southern China (Henan and Jiangxi provinces).

The drought severity showed similar trends with drought duration, indicating that longer drought events corresponded to more severe drought events. Significant decreasing (drying) trends were detected over southwestern China for the ESA CCI SM, while the GLDAS-Noah SM showed decreasing trends over northeastern China, east Inner Mongolia, and parts of the central and southern China. Except for Inner Mongolia and Henan provinces, other regions with drying trends are either humid or semi-humid regions. Over the study period, most parts of northwestern China showed a wetting trend both for ESA CCI

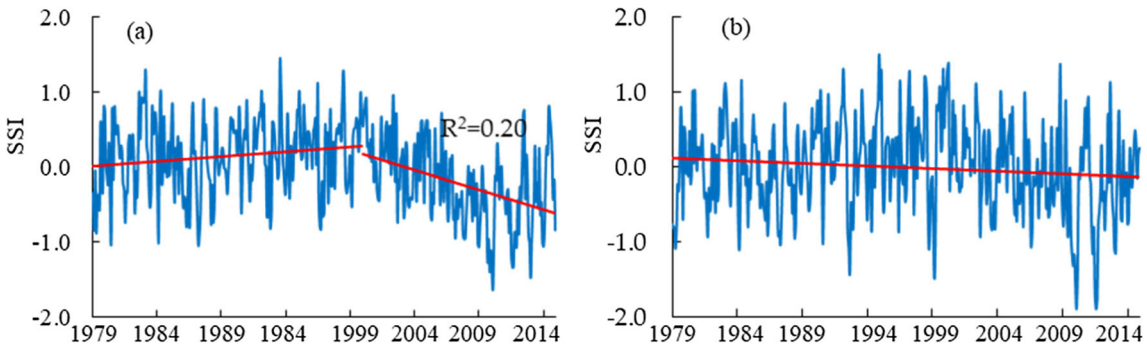

Fig. 8 Averaged monthly SSI changes over southwest China (Yunnan, Sichuan, Guizhou, and south Tibet) from 1979 to 2014 for ESA CCI SM (**a**) and GLDAS SM (**b**)

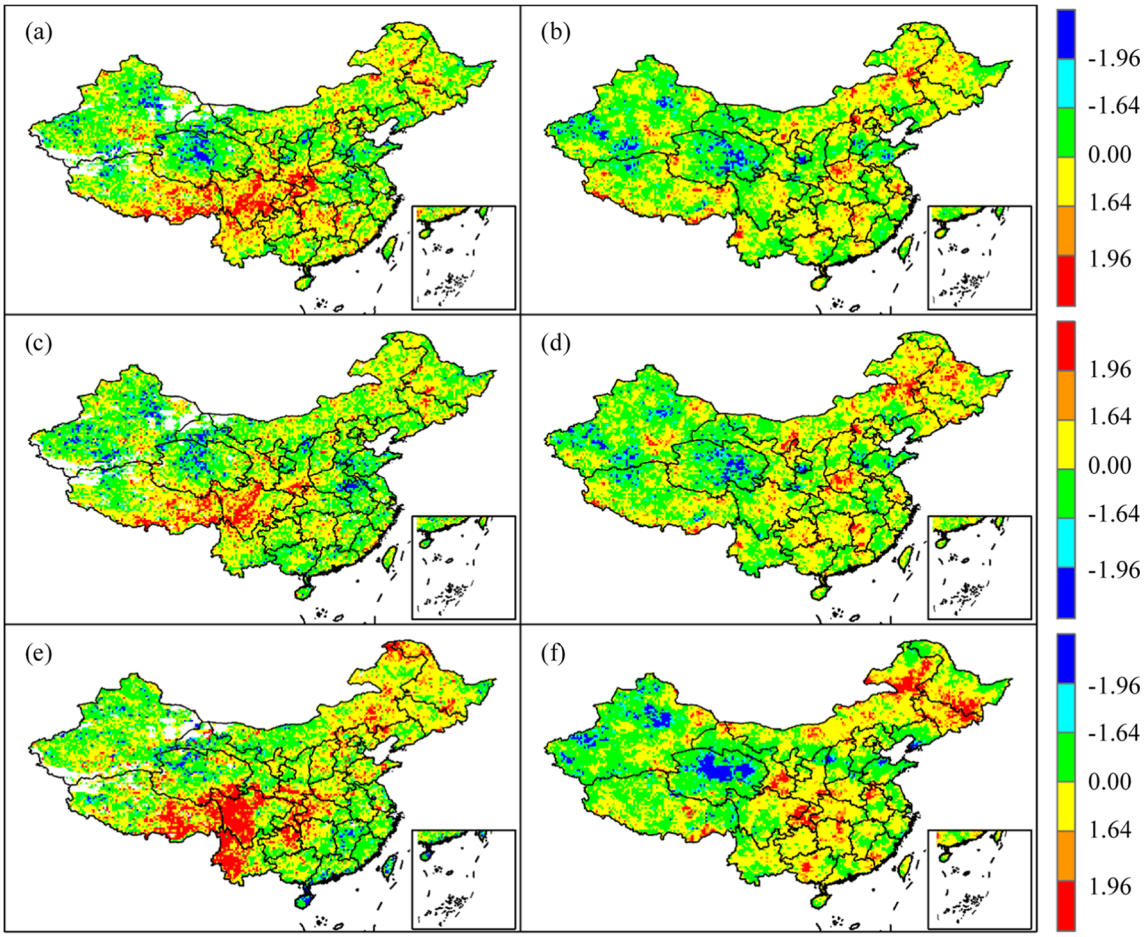

Fig. 9 Spatial distribution of trend significance (M-K z-score) in drought duration, severity, and frequency for ESA CCI SM (**a**, **c**, **e**) and GLDAS SM (**b**, **d**, **f**) over 1979–2014

SM and GLDAS-Noah SM datasets, which was found to be consistent with previous studies (Peng and Zhou 2017).

For the trend significance in drought frequency (Fig. 9e, f), both recorded drying trends (z-score > 1.96) over some parts of northeastern and central China. Concerning the difference, the ESA CCI SM had more regions of increasing drought frequency than the GLDAS-Noah SM in southwestern China. Conversely, the GLDAS-Noah SM had more remarkable wetting trends than the ESA CCI SM, especially in northwestern China (Xinjiang and Qinghai provinces). The discrepancies between ESA CCI and GLDAS-Noah in drought trend detection stress the uncertainties in satellite-derived SM and LSM-modeled SM for drought identification (Seneviratne 2012; Sheffield et al. 2012). The differences are ascribed to the disturbances for satellite retrieval and LSM modeling, for instance, dense vegetation in southern humid China and freeze-thaw surface in northeastern China and Tibetan Plateau.

4.4 Comparison with historical drought events

To verify the quality of these two SM datasets for drought monitoring over China, the SPI-1 data computed using monthly grid precipitation data were used. Three drought events were selected for comparison, including the 2009/2010 southwestern drought (Fig. 10a, b, c), the 2013 southern drought (Fig. 10d, e, f), and the 2007 northern drought (Fig. 10g, h, i).

The extreme drought events extending from autumn 2009 to spring 2010 over southwestern China were the driest event, having the lowest percentage of rainfall anomaly and the longest non-raining days during the winter season in the past 50 years (Yang et al. 2011). This event was the most severe, having the lowest percentage rainfall anomaly in the same period since 1880 (Yang et al. 2011), causing serious economic losses (nearly US$30 billion). The SPI showed that drought centers were located in Guangxi, Guizhou, and Hunan provinces. ESA CCI and GLDAS-Noah also captured spatial patterns of this event; however, they overestimated the severity in Yunnan province and Tibetan Plateau. Specifically, the SPI-1 categorized the drought as moderate and mild drought, while the ESA CCI and GLDAS-Noah classified it as severe, especially for GLDAS-Noah. These discrepancies could be ascribed to high altitude and sparse hydro-meteorological stations, which increased the uncertainty of LSM modeling.

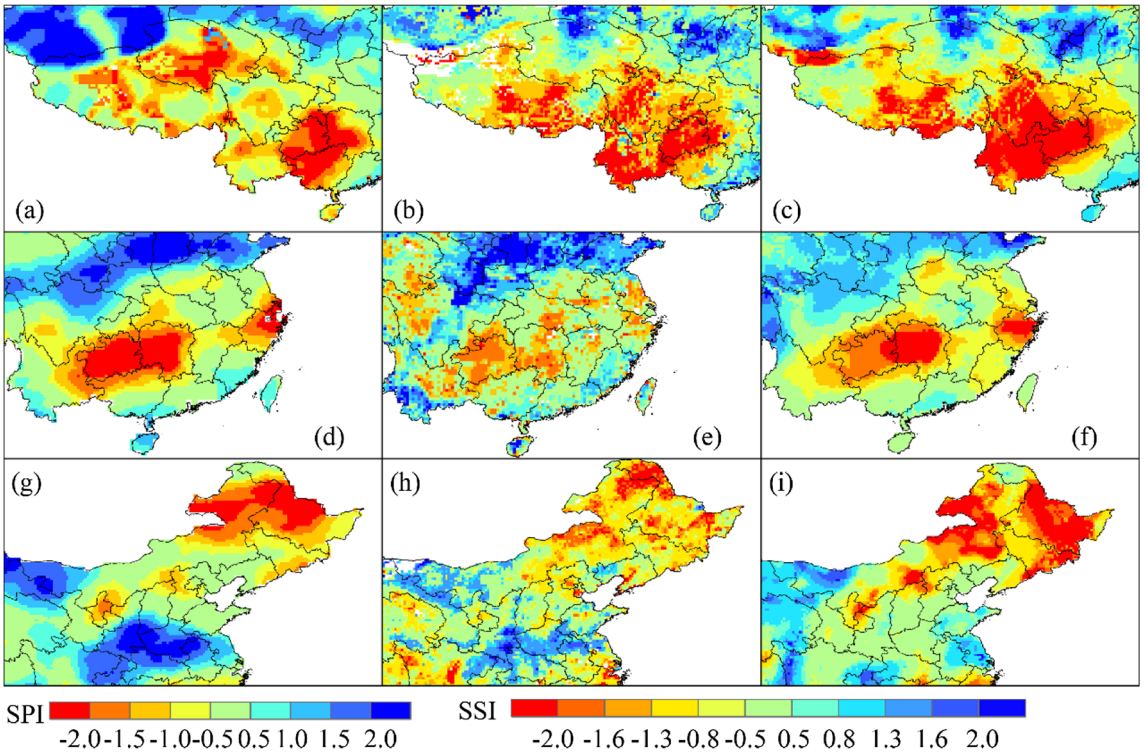

Fig. 10 Extreme drought events detected from the grid precipitation (**a**, **d**, **g**), the GLDAS-Noah (**b**, **e**, **h**), and the ESA CCI (**c**, **f**, **i**) soil moisture. (**a**, **b**, **c**) The drought in February 2010 in southwestern China; (**d**, **e**, **f**) the drought in July 2013 in southern China; and (**g**, **h**, **i**) the drought in July 2007 in northern China

Drought events over southern China in July 2013 were caused by a strong west Pacific subtropical high that extended to the north from its normal position. As shown in the SPI-1 plot (Fig. 10d), the huge drought centers were located in Guizhou, Hunan, and Zhejiang provinces. The GLDAS-Noah perfectly captured the event and thus classified it as a severe drought, which was the same as SPI-1. Comparatively, the ESA CCI displayed similar spatial patterns with a smaller extent and lower severity, especially in Zhejiang province. This may be associated with the dense vegetation over these regions, which compromised the accuracy of satellite SM (Albergel et al. 2013).

In 2007, there was a widespread drought in parts of northern and northeastern China. As displayed in Fig. 10g, the severe drought attacked most of the Heilongjiang province and eastern Inner Mongolia. The ESA CCI dataset displayed a similar pattern with grid precipitation, but with relatively low severity. However, the GLDAS-Noah dataset displayed a larger spatial drought extent, with higher severity. In central China (south Shaanxi, Henan, and Hubei provinces), northern Gansu province, and western Inner Mongolia, the grid precipitation-based SPI-1 showed a wetting trend. The ESA CCI dataset successfully monitored this status, while the GLDAS-Noah dataset failed to detect the wetting pattern. Overall, in central and northern China, the ESA CCI dataset outperforms the GLDAS-Noah dataset in extreme droughts monitoring.

5 Conclusions

ESA CCI SM and GLDAS-Noah soil moisture data were analyzed for drought identification and monitoring over 1979–2014 using SSI. Our results show that large regions of significant correlations between ESA CCI SSI and GLDAS-Noah SSI, indicating high consistency between the two datasets.

Both SM datasets display a similar pattern in drought duration, severity, and frequency. Generally, more severe droughts are found in the arid regions than in humid regions. Also, both SM datasets show a similar trend in drought variations of SSI, and significant drying trends were concentrated in arid regions. However, the two datasets also present a disparity in trends, especially in the Tibet Plateau regions.

To verify the capabilities of the two soil moisture datasets in drought monitoring, three extreme droughts were selected for comparison, and the grid precipitation-based SPI-1 was generated for comparison. It is demonstrated that the two datasets are capable of detecting and describing the spatial pattern of large-scale drought events. However, some discrepancies existed regarding drought severity and drought centers. The ESA CCI dataset is not efficient in south China with dense vegetation, while the GLDAS-Noah dataset is relatively incapable of detecting drought in high altitude and latitude regions. It is also demonstrated that the ESA CCI SM is more robust in delimiting the spatial pattern in the arid regions,

while the GLDAS-Noah SM performed better in the humid and regions.

ESA CCI SM and GLDAS-Noah exhibit high consistencies in spatial patterns, also showing their potentials in drought monitoring across China. However, a substantial discrepancy exists between the two datasets, particularly over high altitude and latitude regions. In the future, multisource data assimilation could be an effective method for drought research.

Code availability The codes for calculating SPI and SSI can be accessed through R package *Drought* (CRAN.R-project.org/package=drought).

Author contributions Gengxi Zhang analyzed the data and wrote the manuscript. Xiaoling Su provided guidance and revised the manuscript. Olusola O. Ayantobo and Kai Feng revised the manuscript and improved grammar.

Funding This work is financially supported by the National Natural Science Foundation of China (grant numbers 51879222 and 52079111) and the China Scholarship Council (201906300059).

Data Availability The data that support the findings of this study are openly available at http://www.esasoilmoisture-cci.org, disc.gsfc.nasa.gov/datasets/, and http://data.cma.cn/.

Declarations

Conflicts of interest The authors declare no competing interests.

References

AghaKouchak A (2014) A baseline probabilistic drought forecasting framework using standardized soil moisture index: Application to the 2012 United States drought. Hydrol Earth Syst Sci 18(7):2485–2492. https://doi.org/10.5194/hess-18-2485-2014

Albergel C, Dorigo W, Reichle RH, Balsamo G, De-Rosnay P, Munoz-Sabater J, Isaksen L, De-Jeu R, Wagner W (2013) Skill and global trend analysis of soil moisture from reanalyses and microwave remote sensing. J Hydrometeorol 14(4):1259–1277. https://doi.org/10.1175/jhm-d-12-0161.1

Al-Yaari A, Wigneron JP, Dorigo W, Colliander A, Pellarin T, Hahn S, Mialon A, Richaume P, Fernandez-Moran R, Fan L, Kerr YH, De-Lannoy G (2019) Assessment and inter-comparison of recently developed/reprocessed microwave satellite soil moisture products using ISMN ground-based measurements. Remote Sens Environ 224:289–303. https://doi.org/10.1016/j.rse.2019.02.008

Ayantobo OO, Wei J (2019) Appraising regional multi-category and multi-scalar drought monitoring using standardized moisture anomaly index (SZI): A water-energy balance approach. J Hydrol 579:124–139. https://doi.org/10.1016/j.jhydrol.2019.124139

Ayantobo OO, Li Y, Song S, Yao N (2017) Spatial comparability of drought characteristics and related return periods in mainland China over 1961–2013. J Hydrol 550:549–567. https://doi.org/10.1016/j.jhydrol.2017.05.019

Beaudoing H, Rodell M (2019) GLDAS Noah land surface model L4 monthly 0.25 x 0.25 degree V2.0, Greenbelt, Maryland, USA, Goddard Earth Sciences Data and Information Services Center (GES DISC), Accessed: [April 20, 2020]. https://doi.org/10.5067/9SQ1B3ZXP2C5

Blyverket J, Hamer PD, Schneider P, Albergel C, Lahoz WA (2019) Monitoring soil moisture drought over northern high latitudes from space. Remote Sens 11(10):1–18. https://doi.org/10.3390/rs11101200

Brocca L, Hasenauer S, Lacava T, Melone F, Moramarco F, Wagner W, Dorigo W, Matgen P, Martínez-Fernández J, Llorens P, Latron J, Martin C, Bittelli M (2011) Soil moisture estimation through ASCAT and AMSR-E sensors: An intercomparison and validation study across Europe. Remote Sens Environ 115(12):3390–3408. https://doi.org/10.1016/j.rse.2011.08.003

Chen S, Gan TY, Tan X, Shao D, Zhu J (2019) Assessment of CFSR, ERA-Interim, JRA-55, MERRA-2, NCEP-2 reanalysis data for drought analysis over China. Clim. Dyn 53(1-2):737–757. https://doi.org/10.1007/s00382-018-04611-1

Dorigo W, de Jeu R, Chung D, Parinussa R, Liu Y, Wagner W, Fernández-Prieto D (2012) Evaluating global trends (1988-2010) in harmonized multi-satellite surface soil moisture. Geophys Res Lett 39(18):1–7. https://doi.org/10.1029/2012gl052988

Dorigo WA, Gruber A, De-Jeu RAM, Wagner W, Stacke T, Loew A, Albergel C, Brocca L, Chung D, Parinussa RM, Kidd R (2015) Evaluation of the ESA CCI soil moisture product using ground-based observations. Remote Sens Environ 162:380–395. https://doi.org/10.1016/j.rse.2014.07.023

Dorigo W, Wagner W, Albergel C, Albrecht F, Balsamo G, Brocca L, Chung D, Ertl M, Forkel M, Gruber A, Haas E, Hamer PD, Hirschi M, Ikonen J, de Jeu R, Kidd R, Lahoz W, Liu YY, Miralles D, Mistelbauer T, Nicolai-Shaw N, Parinussa R, Pratola C, Reimer C, van der Schalie R, Seneviratne SI, Smolander T, Lecomte P (2017) ESA CCI soil moisture for improved earth system understanding: State-of-the art and future directions. Remote Sens Environ 203:185–215. https://doi.org/10.1016/j.rse.2017.07.001

Drusch M (2005) Observation operators for the direct assimilation of TRMM microwave imager retrieved soil moisture. Geophys Res Lett 32(15):1–4. https://doi.org/10.1029/2005gl023623

Entekhabi D, Njoku EG, O'Neill PE, Kellogg KH, Crow WT, Edelstein WN, Entin JK, Goodman SD, Jackson TJ, Johnson J, Kimball J, Piepmeier JR, Koster RD, Martin N, McDonald KC, Moghaddam M, Moran S, Reichle R, Shi JC, Spencer MW, Thurman SW, Tsang L, van Zyl J (2010) The Soil Moisture Active Passive (SMAP) Mission. Proc IEEE 98(5):704–716. https://doi.org/10.1109/JPROC.2010.2043918

Fang L, Hain CR, Zhan X, Anderson MC (2016) An inter-comparison of soil moisture data products from satellite remote sensing and a land surface model. Int J Appl Earth Obs Geoinf 48:37–50. https://doi.org/10.1016/j.jag.2015.10.006

Ferguson CR, Wood EF (2011) Observed land–atmosphere coupling from satellite remote sensing and reanalysis. J Hydrometeorol 12(6):1221–1254. https://doi.org/10.1175/2011jhm1380.1

Gringorten II (1963) A plotting rule for extreme probability paper. J Hydrometeorol 68:813–814. https://doi.org/10.1029/JZ068i003p00813

Hao Z, AghaKouchak A (2013) Multivariate standardized drought index: A parametric multi-index model. Adv Water Resour 57:12–18. https://doi.org/10.1016/j.advwatres.2013.03.009

Hao Z, Singh VP (2015) Drought characterization from a multivariate perspective: A review. J Hydrol 527:668–678. https://doi.org/10.1016/j.jhydrol.2015.05.031

Hao Z, AghaKouchak A, Nakhjiri N, Farahmand A (2014) Global integrated drought monitoring and prediction system. Sci Data 1:1–10. https://doi.org/10.1038/sdata.2014.1

Jin D, Guan Z, Tang W (2013) The extreme drought event during winter–spring of 2011 in East China: Combined influences of teleconnection in midhigh latitudes and thermal forcing in

Maritime continent region. J Clim 26(20):8210–8222. https://doi.org/10.1175/jcli-d-12-00652.1
Kerr YH, Waldteufel P, Wigneron JP, Martinuzzi JM, Font J, Berger M (2001) Soil moisture retrieval from space: the Soil Moisture and Ocean Salinity (SMOS) Mission. IEEE Trans Geosci Remote Sensing 39(8):1729–1735. https://doi.org/10.1109/36.942551
Levine PA, Randerson JT, Swenson SC, Lawrence DM (2016) Evaluating the strength of the land– atmosphere moisture feedback in Earth system models using satellite observations. Hydrol Earth Syst Sci 20(12):4837–4856. https://doi.org/10.5194/hess-20-4837-2016
Liu YY, Dorigo WA, Parinussa RM, De-Jeu RAM, Wagner W, McCabe MF, Evans JP, van Dijk AIJM (2012) Trend-preserving blending of passive and active microwave soil moisture retrievals. Remote Sens Environ 123:280–297. https://doi.org/10.1016/j.rse.2012.03.014
Liu YW, Wang W, Hu YM, Liang ZM (2014) Drought assessment and uncertainty analysis for Dapoling basin. Nat Hazards 74(3):1613–1627. https://doi.org/10.1007/s11069-014-1259-4
Liu M, Xu X, Sun AY, Wang K (2017) Decreasing spatial variability of drought in southwest China during 1959-2013. Int J Climatol 37(13):4610–4619. https://doi.org/10.1002/joc.5109
Liu Y, Liu Y, Wang W (2019) Inter-comparison of satellite-retrieved and Global Land Data Assimilation System-simulated soil moisture datasets for global drought analysis. Remote Sens Environ 220:1–18. https://doi.org/10.1016/j.rse.2018.10.026
Lloyd-Hughes B, Saunders MA (2002) A drought climatology for Europe. Int J Climatol 22(13):1571–1592. https://doi.org/10.1002/joc.846
Mckee TB, Doesken NJ, Kleist J (1993) The relationship of drought frequency and duration to time scales, Eighth Conference on Applied Climatology American Meteorology Society, Anaheim, pp. 17-22.
McVicar TR, Jupp DLB (1998) The current and potential operational uses of remote sensing to aid decisions on drought exceptional circumstances in Australia: A review. Agric Syst 57(3):399–468. https://doi.org/10.1016/S0308-521X(98)00026-2
Mo KC, Lettenmaier DP (2014) Objective drought classification using multiple land surface models. J Hydrometeorol 15(3):990–1010
Peng D, Zhou T (2017) Why was the arid and semiarid northwest China getting wetter in the recent decades? J Geophys Res-Atmos 122(17):9060–9075. https://doi.org/10.1002/2016jd026424
Rajasekaran E, Das N, Poulsen C, Behrangi A, Swigart J, Svoboda M, Entekhabi D, Yueh S, Doorn B, Entin J (2018) SMAP soil moisture change as an Indicator of drought conditions. Remote Sensing 10(5):788
Raziei T (2017) An analysis of daily and monthly precipitation seasonality and regimes in Iran and the associated changes in 1951–2014. Theor Appl Climatol 134(3-4):913–934. https://doi.org/10.1007/s00704-017-2317-0
Reichle RH (2004) Bias reduction in short records of satellite soil moisture. Geophys Res Lett 31(19):1–4. https://doi.org/10.1029/2004gl020938
Robock A, Vinnikov KY, Srinivasan G, Entin JK, HoIIinger SE, Speranskaya NA, Liu S, Namkhai A (2000) The global soil moisture data bank. Bull Amer Meteorol Soc 81(6):1281–1299
Rodell M, Houser PR, Jambor U, Gottschalck J, Mitchell K, Meng CJ, Arsenault K, Cosgrove B, Radakovich J, Bosilovich M, Entin JK, Walker JP, Lohmann D, Toll D (2004) The global land data assimilation system. Bull Amer Meteorol. Soc 85:381–394. https://doi.org/10.1175/BAMS-85-3-381
Seneviratne SI (2012) Historical drought trends revisited. Nature 491(7424):338–339
Sheffield J, Wood EF, Roderick ML (2012) Little change in global drought over the past 60 years. Nature 491(7424):435–438. https://doi.org/10.1038/nature11575
Sims AP, Niyogi DDS, Raman S (2002) Adopting drought indices for estimating soil moisture: A North Carolina case study. Geophys Res Lett 29(8):24-1-24-4. https://doi.org/10.1029/2001gl013343
Spennemann PC, Rivera JA, Saulo AC, Penalba OC (2015) A comparison of GLDAS soil moisture anomalies against standardized precipitation index and multisatellite estimations over South America. J Hydrometeorol 16(1):158–171. https://doi.org/10.1175/jhm-d-13-0190.1
Szalai S, Szinell CS (2000) Comparison of two drought indices for drought monitoring in Hungary—a case study. In: Drought and Drought Mitigation in Europe. Springer, Netherlands. https://doi.org/10.1007/978-94-015-9472-1_12
Taylor KE, Stouffer RJ, Meehl GA (2012) An overview of CMIP5 and the experiment design. Bull Amer Meteorol Soc 93(4):485–498. https://doi.org/10.1175/bams-d-11-00094.1
Vergopolan N, Chaney NW, Beck HE, Pan M, Sheffield J, Chan S, Wood EF (2020) Combining hyper-resolution land surface modeling with SMAP brightness temperatures to obtain 30-m soil moisture estimates. Remote Sens Environ 242:111740. https://doi.org/10.1016/j.rse.2020.111740
Wang W, Cui W, Wang X, Chen X (2016) Evaluation of GLDAS-1 and GLDAS-2 forcing data and Noah model simulations over China at the monthly scale. J Hydrometeorol 17(11):2815–2833. https://doi.org/10.1175/jhm-d-15-0191.1
Wilhite DA, Glantz MH (1985) Understanding: the drought phenomenon: the role of definitions. Water Int 10(3):111–120. https://doi.org/10.1080/02508068508686328
Yang J, Gong D, Wang W, Hu M, Mao R (2011) Extreme drought event of 2009/2010 over southwestern China. Meteorol Atmos Phys 115(3-4):173–184. https://doi.org/10.1007/s00703-011-0172-6
Yang Y, Gan TY, Tan X (2020) Spatiotemporal changes of drought characteristics and their dynamic drivers in Canada. Atmos Res 232:104695. https://doi.org/10.1016/j.atmosres.2019.104695
Yuan X, Ma Z, Pan M, Shi C (2015) Microwave remote sensing of short-term droughts during crop growing seasons. Geophys Res Lett 42(11):4394–4401. https://doi.org/10.1002/2015gl064125
Zhang L, Xiao J, Li J, Wang K, Lei L, Guo H (2012) The 2010 spring drought reduced primary productivity in southwestern China. Environ Res Lett 7(4):045706. https://doi.org/10.1088/1748-9326/7/4/045706
Zhang B, Kouchak AA, Yang Y, Wei J, Wang G (2019a) A water-energy balance approach for multi-category drought assessment across globally diverse hydrological basins. Agric For Meteorol 264:247–265. https://doi.org/10.1016/j.agrformet.2018.10.010
Zhang L, Liu Y, Ren L, Jiang S, Yang X, Yuan F, Wang M, Wei L (2019b) Drought monitoring and evaluation by ESA CCI soil moisture products over the Yellow River Basin. IEEE J Sel Top Appl Earth Observ Remote Sens 12(9):3376–3386. https://doi.org/10.1109/jstars.2019.2934732
Zhao Y, Zhu J, Xu Y (2014) Establishment and assessment of the grid precipitation datasets in China for the past 50 years. J Meteorol Sci 34(4):414–420 (in Chinese with English abstract)
Zwieback S, Paulik C, Wagner W (2015) Frozen soil detection based on advanced scatterometer observations and air temperature data as part of soil moisture retrieval. Remote Sens 7(3):3206–3231. https://doi.org/10.3390/rs70303206